**RC22723 (W0302-051) February 13, 2003**
**Materials Science**

# IBM Research Report

## Effects of Phosphorus Content on the Reaction of Electroless Ni-P with Sn and Crystallication of Ni-P

**Y. C. Sohn , Jin Yu**
Dept. of Materials Science and Engineering,
Korea Advanced Institute of Science and Technology
373-1 Kusong-dong, Yusong-gu, Daejon, Korea

**Sung K. Kang, Da-Yuan Shih**
IBM Research Division
Thomas J. Watson Research Center
P.O. Box 218
Yorktown Heights, NY 10598

**W. K. Choi**
Materials & Device Lab.,
Samsung Advanced Institute of Technology,
P.O.Box 111, Suwon 440-600, Korea

**Research Division**
**Almaden - Austin - Beijing - Delhi - Haifa - India - T. J. Watson - Tokyo - Zurich**

# Effects of Phosphorus Content on the Reaction of Electroless Ni-P with Sn and Crystallization of Ni-P

**Y. C. Sohn (sonyc@kaist.ac.kr) and Jin Yu**

Dept. of Materials Science and Engineering,

Korea Advanced Institute of Science and Technology

373-1 Kusong-dong, Yusong-gu, Daejon, Korea

**S. K. Kang and D. Y. Shih**

IBM T. J. Watson Research Center,

P.O.Box 218/Route 134, Yorktown Heights, NY 10598

**W. K. Choi**

Materials & Device Lab., Samsung Advanced Institute of Technology,

P.O.Box 111, Suwon 440-600, Korea

## ABSTRACT

The reaction between electroless Ni-P and Sn, and the crystallization behavior of Ni-P were investigated to better understand the effect of the P content of the Ni-P layer. Electroless Ni-P specimens with three different P contents, 4.6, 9 and 13wt%, were used to study the effect of P content and microstructure of Ni-P on the subsequent crystallization and IMC formation during the reaction between Ni-P and electroplated Sn. $Ni_3Sn_4$ was the major phase formed in all samples heated up to 300°C, which totally transformed into $Ni_3Sn_2$ when samples were heated up to 450°C and the Sn layer was 0.5μm thick. The IMC formed on the nanocrystalline Ni-P showed stronger texture compared to that formed on the amorphous Ni-P. Both the IMC thickness and density decreased with the P content in the Ni-P layer and $Ni_3Sn_4$ morphologies varied with the P content. Dissolution of Ni into Sn increased with the P content, which made IMC size in the bulk Sn increase with the P content.

## INTRODUCTION

Electroless nickel-phosphorus (Ni-P) film is widely used for under bump metallization (UBM) for flip chip and substrate metallizations for ball grid array (BGA) applications in microelectronic industry. This is due to its superior characteristics such as excellent solderability, corrosion resistance, uniform thickness and selective deposition.[1-5]

The microstructure of a Ni-P film changes significantly with its P content. A Ni-P layer containing less than 5.5 wt.% P is known to be nanocrystalline, while that of more than 9 wt.% P is amorphous.[6,7] Ni-P films with 5.5~8.5 wt.% P are known to be a mixture of small crystallites and an amorphous phase.[8] A transition point to an amorphous structure is not clear since Ni-P with 10.1 wt.% P was reported to have 4~5nm grains even though its electron diffraction pattern showed amorphous characteristics.[9] The crystallization temperature of a Ni-P film is also known to vary widely depending on P content ; 300~450°C for 1.9~13.6 wt.% P.[9-11]

When a Ni-P film reacts with Sn-Pb eutectic solder, some part of the film underneath the solder crystallizes into $Ni_3P$ (P-rich layer) around the reflow temperature (200~240°C). This low temperature reaction is called as "solder reaction-assisted crystallization"[12], in contrast to the self-crystallization of Ni-P at a higher temperature. The solder reaction-assisted crystallization is accompanied with the formation of Ni-Sn intermetallic compound (IMC) and Kirkendall voids.[13,14] This interfacial reactions are often attributed to form a weak and brittle interface between Ni-P and Sn-Pb solder[1,2,5].

When Sn-Pb solder is replaced by Sn-rich Pb-free solders, the reliability issue of the Ni-P interface is expected to be even more important since Pb-free solders have a higher Sn content and a higher reflow temperature.[4,15] Hence, a detailed study on the reaction mechanism between electroless Ni-P and Sn as well as the self-crystallization of Ni-P is

required to better understand the reliability issues associated with Ni-P ball limiting metallization (BLM). In this study, the effects of P content on the solder reaction-assisted crystallization, intermetallic compound formation, and self-crystallization of Ni-P have been therefore investigated by choosing three different levels of P content (low, medium and high) as a major variable.

## EXPERIMENTAL PROCEDURE

A Cu foil of 25 μm was used as a substrate, which was cleaned with acetone and treated in a 0.5M $H_2SO_4$ solution to remove surface oxides. The Cu foil was then activated with a Pd solution before electroless Ni-P plating. Nine micron thick Ni-P layer with the P content of 4.6, 9, and 13wt% was electrolessly deposited with EN 1400, EN 9185, and EN 3600 solution products of Technic Inc. Cranston, RI, respectively on the Cu foil. It was followed by an electrodeposition of a Sn layer of 0.5~5 μm with Solderon SC solution (from Shipley company, Marlborough, MA) at a current density of 37.5 mA/cm$^2$.

The P content in the Ni-P layer was analyzed by an electron probe microanalyzer (EPMA). The microstructure of Ni-P is expected to vary depending on the P content; nanocrystalline for 4.6 wt% P, amorphous with some crystallites for 9 wt% P, and completely amorphous for 13 wt%.[6-10]

Differential scanning calorimetry (DSC) was used to study the interfacial reaction between Ni-P and Sn and the crystallization of Ni-P at a heating rate of 5°C/min in $N_2$ atmosphere. Samples heated to 300 and 450°C in the DSC were cooled down in air to room temperature and the remaining Sn after reaction was etched with 10 vol% HCl solution. To prepare a cross-sectional view, the reflowed samples were mounted using

epoxy and then prepared metallographically to a final finish of 0.05μm using alumina slurry. The surface of polished samples was etched with 3%HCl-5%$HNO_3$-92%$CH_3OH$ (in vol%) solution for several minutes. X-ray diffraction (XRD) analysis with Cu Ka radiation was performed to identify the crystalline structure of each sample, and scanning electron microscopy (SEM) was used for the microstructural analysis.

To demonstrate the reaction of Ni-P with a practical solder volume used in reflow soldering, 120μm thick Sn layer was electroplated on 9μm thick Ni-P film of varying P content (4.6, 9, 13 wt%) and reflowed at 250°C for 1, 2, and 10 min in $N_2$ atmosphere. The Ni-P films denoted as Ni-4.6P, Ni-9P and Ni-13P specimens after their P content in the film.

## RESULTS AND DISCUSSION

### A. Thermal Analysis by DSC

Figure 1 shows DSC curves of 9μm thick Ni-9P films with Sn layers of varying thickness (0.5~5μm) which were heated up to 450°C with a heating rate of 5°C/min. The Ni-9P sample without Sn layer (top curve) showed a typical self-crystallization peak around 340°C, where Ni-9P transformed into $Ni_3P$ and crystalline Ni. With a Sn layer present on the Ni9-P film, a broad exothermic peak of $Ni_3Sn_4$ was detected at 190~250°C, which increased gradually with the Sn thickness. In addition, a sharp endothermic peak of Sn melting around 232°C was superposed with the $Ni_3Sn_4$ peak when an excessive Sn was available as shown for the 5μm Sn sample. A detailed analysis of the crystallization process was published elsewhere.[16] To isolate the reaction at low temperatures from the self-crystallization at high temperatures, some samples were heated only up to 300°C and

cooled to room temperature in air.

DSC curves of Ni-4.6P, Ni-9P and Ni-13P films without Sn and their heat of crystallization measured from the curves are presented in Fig. 2 as a function of the P content. The crystallization temperature of the Ni-P films were higher than 300°C in all cases, but decreased with P content in the film, which was consistent with the previous report[17]. The heat of crystallization of Ni-P was estimated by measuring the area of exothermic peaks and applying the following relation;

$$\frac{\Delta H(\textit{heat measured by DSC})}{\Delta H(\textit{heat of crystalliz ation}, Ni-P)} = \frac{r(Ni-P)V(Ni-P)}{r(Sn)V(Sn)+r(Ni-P)V(Ni-P)+r(Cu)V(Cu)} \qquad (1)$$

Here, $?H_{meas}$ and $?H_{Ni\text{-}P}$ refer to measured heat from the Cu/Ni-P/Sn sample and the heat of crystallization of Ni-P per gram, and ? and V denote the density and volume, respectively. Deduced heat of crystallization of Ni-P per gram is presented in Fig. 2 (b), and it can be seen that the heat of crystallization increased almost linearly with the P content in the Ni-P film. Since Ni-P was deposited as a metastable state, the driving force to transform into crystalline Ni and $Ni_3P$ phases tends to increase with the amorphousness in the film which can be related to the P content in the Ni-P film.

**B. X-ray Diffraction Analysis for Phase Identification**

Figure 3 is a collection of XRD patterns out of Ni-4.6P, Ni-9P and Ni-13P films (9μm thick) reacted with Sn layers of varying thickness (0.5~2μm). To distinguish the solder reaction-assisted crystallization from the self-crystallization at high temperature, the samples were heated up to 300°C or 450°C in two different groups. For samples heat-treated up to 300°C, a small broad Ni (111) peak was found for the medium and high P

content in Fig. 3(b) and Fig. 3(c), indicating the presence of an amorphous Ni-P phase even after the heat treatment. In the case of Ni-4.6P samples, Fig.3(a), the Ni peak was much larger as shown in Fig. 3(a), implying higher degree of crystallinity than Ni-9P or Ni-13P specimens.

When the Ni-P films coated with Sn heated up to 300°C, $Ni_3Sn_4$ was found in all samples. Since the intensity of the $Ni_3Sn_4$ peaks were much larger in the Ni-4.6P specimen than in the Ni-9P or Ni-13P specimens, it can be seen that the formation of $Ni_3Sn_4$ IMC was strongly affected by the P content in the Ni-P film, which will be discussed further in the next section.

For Ni-P samples heated up to 450°C, Ni-P phase is known to transform into crystalline Ni and $Ni_3P$ phases completely[9,10], which is consistent with what was observed in Fig. 3(d), (e) and (f). Note that Ni (111) peak decreased with the P content as in the case of specimens heated up to 300°C. When the thickness of Sn was 0.5 μm, only $Ni_3Sn_2$ was found, while both $Ni_3Sn_4$ and $Ni_3Sn_2$ were present in the samples with more than 1 μm Sn. Again, the peak intensities of $Ni_3Sn_4$ IMCs were smaller for the samples with higher P content. During heating up to 450°C, $Ni_3Sn_4$ nucleated and grew initially but subsequently coalesced into $Ni_3Sn_2$, which is consistent with previous reports.[18,19]

For fully crystallized Ni-P samples without Sn shown in Fig. 3(d), (e), and (f), Ni (200) peak of Ni-4.6P sample was much smaller than that of Ni-9P or Ni-13P specimens. Thus, it appears that nanocrystalline Ni-P more or less maintains its initial (111) texture during the subsequent phase transformation, while new texture with various orientation evolved in case of amorphous Ni-P.[9] It is interesting to note that $Ni_3Sn_4$ IMC formed in Ni-4.6P samples also showed stronger (111) texture than that in higher P specimens, which suggests that the texture of $Ni_3Sn_4$ IMC was affected by that of pre-existing Ni

crystallites.

### C. Effect of P Content on Ni-Sn Intermetallics

Fig. 4 shows various morphologies of Ni-Sn IMCs formed at Ni-P/Sn interfaces. After the heating experiment, unreacted Sn was removed by etching and SEM micrographs were taken from the top surface of a reacted sample. The $Ni_3Sn_4$ IMCs formed in Ni-4.6P and Ni-13P specimens heated to 300°C revealed a faceted column-like morphology with faceted or broken tip as shown in Fig. 4(a) and (b). The $Ni_3Sn_4$ found in a low P content sample is more densely packed and more faceted than the others. This is consistent with the XRD observation of different intensities of $Ni_3Sn_4$ among specimens with different P content.

Samples with Sn 0.5μm heated to 450°C revealed the presence of $Ni_3Sn_2$ IMC which showed a faceted and chunky-type morphology as shown in Fig. 4(c). Generally, $Ni_3Sn_2$ is known to form underneath $Ni_3Sn_4$[14,18], which makes it difficult to observe the morphology of $Ni_3Sn_2$, however small amount of Sn available made $Ni_3Sn_2$ form directly on Ni-P in the present case.

Cross-sectional SEM micrographs of 9μm thick Ni-4.6P and Ni-9P specimens with 2μm thick Sn heated up to 300°C are shown in Fig. 5. The average thickness of $Ni_3Sn_4$ and P-rich layer are measured and plotted in Fig. 5(c). It can be seen that the growth of $Ni_3Sn_4$ is more affected by the thickness of Sn layer than by the P content in the Ni-P layer, while the reverse is true of the P-rich layer. For example, Ni-4.6P samples showed the thickest IMC layer and the thinnest P-rich layer, simultaneously, which is consistent with the XRD analysis where the Ni-4.6P specimen showed the largest Ni-Sn IMC peaks.

Possible explanations of the fast IMC growth in a low P sample include; more

nucleation sites on the nanocrystalline Ni-P, fast diffusion of Ni atoms through grain boundaries, fast interdiffusion through a thin P-rich layer and others. Some voids are observed in the P-rich layers of the samples, which is consistent with what was reported previously.[13]

**D. Reaction of Ni-P with Thick Sn Layer**

In order to understand the interfacial reaction of Ni-P in practical reflow soldering, experiments were conducted by reacting Ni-4.6P, Ni-9P and Ni-13P samples with a thick Sn layer of 120μm. Figure 6 shows the cross-sectional microstructures of 9μm thick Ni-9P and Ni-13P specimens after reaction with 120μm thick Sn at 250°C up to 10 minutes. Resultant thickness of $Ni_3Sn_4$ and P-rich layers were measured and plotted as a function of reflow time in Fig. 6(c). Here, overall thickness of $Ni_3Sn_4$ IMC was much larger than that of thin Sn specimens, however the general trend of IMC thickening being suppressed by the P increase in the Ni-P layer, particularly for the Ni-13P specimen, was consistent with the results of thin Sn samples. The morphology of Ni-Sn IMCs was affected by both P content and reflow time. For a short reflow time such as 1min at 250 °C, the needle-type morphology was observed in all samples. For an extended reflow time such as 10 min, the needle-like IMCs became chunky in the Ni-4.6P and Ni-9P samples, while needle-type IMC still prevailed in the Ni-13P sample.

The Ni-Sn IMCs formed inside the solder during solidification seemed to be affected by the P content in the Ni-P layer; the IMCs were much longer and thicker in the high P sample as can be seen by comparing Fig. 6(a) with 6(b). This enhanced growth of Ni-Sn IMCs in the solder matrix with the P content in the Ni-P layer may be explained by the fact that the interfacial IMCs formed in the high P samples have a needle-type

morphology and porous structure, which provided more Ni dissolution into the solder during reflow. In general, the same trend was observed between the thick and thin Sn samples in terms of the formation of interfacial IMCs and P-rich layer, as well as their dependence on P content.

## CONCLUSIONS

The reaction mechanisms between Ni-P and Sn during reflow soldering were investigated by separating the solder reaction-assisted crystallization of Ni-P from the high temperature self-crystallization. Using Ni-P specimens with electroplated Sn, the solder reaction process was investigated using DSC and XRD techniques, and effects of P content on the crystallization of Ni-P and IMC formation were studied. Conclusions are :

1. The solder reaction-assisted crystallization of Ni-P at a low temperature was confirmed by observing the formation of P-rich layer and Ni-Sn intermetallics.
2. $Ni_3Sn_4$ was the major phase formed in all samples heated to 300°C, while only $Ni_3Sn_2$ was observed when the Sn layer was very thin (0.5μm Sn layer heated to 450°C).
3. The interfacial Ni-Sn IMCs showed strong (111) texture when the P content of the underlying Ni-P layer was low (4.6 wt.% P).
4. The thickness and density of Ni-Sn IMCs formed on Ni-P were strongly affected by the P content of the underlying Ni-P layer; higher P content yields thinner and less densely packed IMCs.
5. Common trends were found between the Ni-P specimens with thin and thick Sn

layers about the effect of P content on the formation of Ni-Sn IMCs and P-rich layer. The IMC thickness decreased with the P content of the underlying Ni-P layer, while the thickness of P-rich layer grew in the opposite way.

6. Dissolution of Ni into Sn increased with the P content in the Ni-P layer, which made IMCs in the bulk Sn increase with the P content.

## Acknowledgements

This work was supported by the Center for Electronic Packaging Materials at KAIST funded by Korea Science and Engineering Foundation. Y. C. Sohn was supported by the Brain Korea 21 program during his stay at IBM T. J. Watson Research Center under the KAIST-IBM joint study program.

## References

1. S. Wiegele, P. Thompson, R. Lee and E. Ramsland, Proceedings of IEEE Electronic Component and Technology Conference, 1998, p. 861.
2. Z. Mei, M. Kaufmann, A. Eslambolchi and P. Johnson, Proceedings of IEEE Electronic Component and Technology Conference, 1998, p. 952.
3. J. K. Lin, A. D. Silva, D. Frear, Y. Guo, J. W. Jang, L. Li, D. Mitchell, B. Yeung and C. Zhang, Proceedings of IEEE Electronic Component and Technology Conference, 2001, p. 455.

4. M. O. Alam, Y. C. Chan and K. C. Hung, Proceedings of IEEE Electronic Component and Technology Conference, 2002, p. 1650.
5. D. Goyal, T. Lane, P. Kinzie, C. Panichas, K. M. Chong and O. Villalobos, Proceedings of IEEE Electronic Component and Technology Conference, 2002, p. 732.
6. Kreye, H., Müller, F., Lang, K., Isheim, D. and Hentschel, T., Z. Metallkd. **86**, 184 (1995).
7. Kreye, H., Müller, H.-H. and Petzel, T., Galvanotechnik **77**, 561 (1986).
8. Dietz, G. and Schneider, H. D., J. Phys.: Condens. Matter **2**, 2169 (1990).
9. S. H. Park and D. N. Lee, J. Mater. Sci. **23**, 1643 (1988).
10. K. H. Hur, J. H. Jeong and D. N. Lee, J. Mater. Sci. **25**, 2573 (1990).
11. Th. Hentschel, D. Isheim, R. Kirchheim, F. Müller and H. Kreye, Acta Mater. **48**, 933 (2000).
12. J. W. Jang, P. G. Kim, K. N. Tu, D. R. Frear and P. Thompson, J. Appl. Phys. **85**, 8456 (1999).
13. K. C. Hung, Y. C. Chan, C. W. Tang and H. C. Ong, J. Mater. Res. **15**, 2534 (2000).
14. P. L. Liu, Z. Xu and J. K. Shang, Metall. Mater. Trans. A **31A**, 2857 (2000).
15. K. Zeng, K. N. Tu, Materials Science and Engineering **R 38**, 55 (2002).
16. Y. C. Sohn, Jin Yu, S. K. Kang, W. K. Choi and D. Y. Shih, J. Mater. Res. **18**, 4 (2003).
17. M. W. Mahoney and P. J. Dynes, Scripta Metallurgica **19**, 539 (1985).
18. S. K. Kang and V. Ramachandran, Scripta Metallurgica **14**, 421 (1980).
19. C. Y. Lee and K. L. Lin, Thin Solid Films **249**, 201 (1994).

## Figure captions

Fig. 1. DSC curves of 9μm thick Ni-9P reacted with Sn layers of varying thickness (0.5~5μm) which were heated up to 450°C at a heating rate of 5°C/min.

Fig. 2. (a) DSC curves of 9μm thick Ni-4.6P, Ni-9P and Ni-13P films without Sn heated up to 450°C at a heating rate of 5°C/min and (b) Heat of crystallization deduced from the DSC curves as a function of the P content in the Ni-P layer.

Fig. 3. XRD patterns out of 9μm thick Ni-P films reacted with Sn layers of varying thickness (0.5~2μm) heated up to 300°C in case of (a) Ni-4.6P (b) Ni-9P (C) Ni-13P and heated up to 450°C in case of (d) Ni-4.6P (e) Ni-9P (f) Ni-13P at a heating rate of 5°C/min.

Fig. 4. Morphologies of Ni-Sn IMCs formed at Ni-P/Sn interfaces. (a) $Ni_3Sn_4$ formed at 9μm thick Ni-4.6P reacted with 2μm thick Sn layer heated up to 300°C (b) $Ni_3Sn_4$ formed at 9μm thick Ni-13P reacted with 2μm thick Sn layer heated up to 300°C (C) $Ni_3Sn_2$ formed at 9μm thick Ni-13P reacted with 0.5μm thick Sn layer heated up to 450°C at a heating rate of 5°C/min.

Fig. 5. Cross-sectional SEM micrographs of 9μm thick Ni-P reacted with 2μm thick Sn layer heated up to 300°C at a heating rate of 5°C/min in case of (a) Ni-4.6P and (b) Ni-9P and (C) the average thickness of $Ni_3Sn_4$ and P-rich layer as a function of Sn layer thickness.

Fig. 6. Cross-sectional SEM micrographs of 9μm thick Ni-P reacted with 120μm thick Sn layer reflowed at 250°C up to 10 minutes in case of (a) Ni-9P and (b) Ni-13P and (C) the average thickness of $Ni_3Sn_4$ and P-rich layer as a function of reflow time.

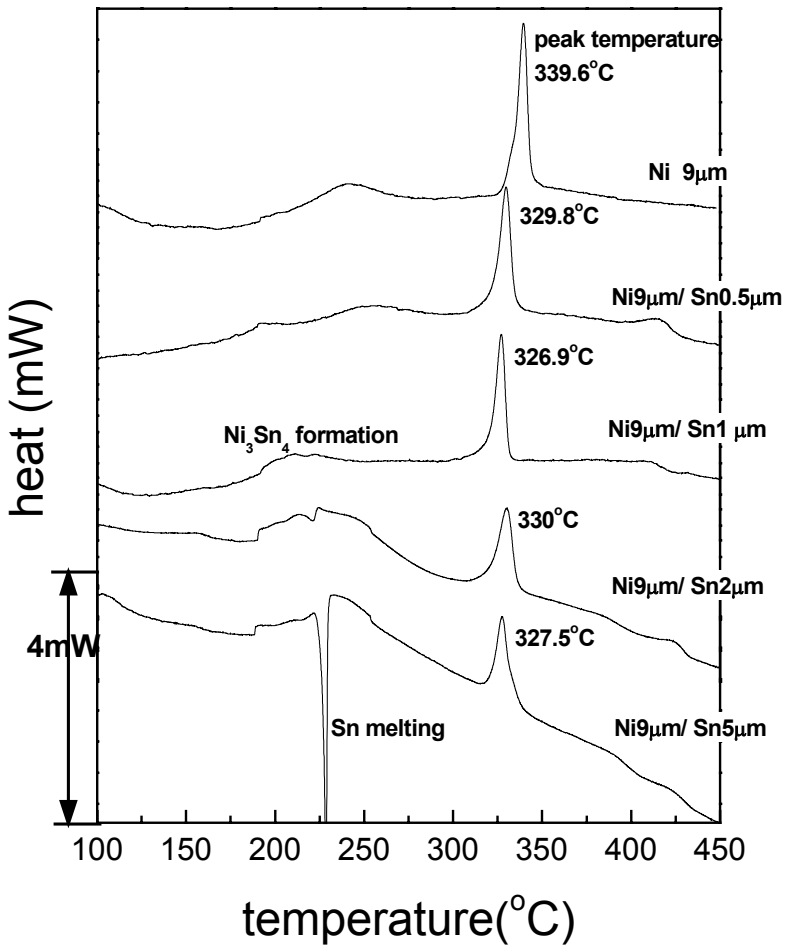


Fig. 1. DSC curves of 9μm thick Ni-9P reacted with Sn layers of varying thickness (0.5~5μm) which were heated up to 450°C at a heating rate of 5°C/min.

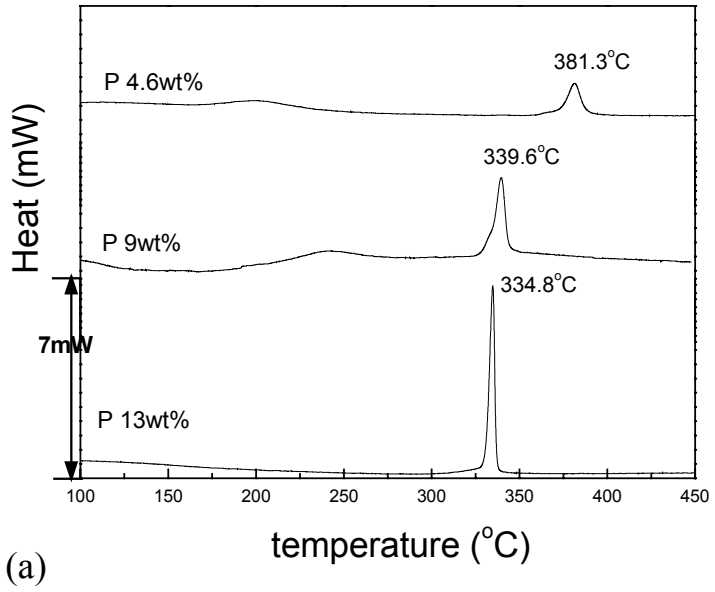


(a)

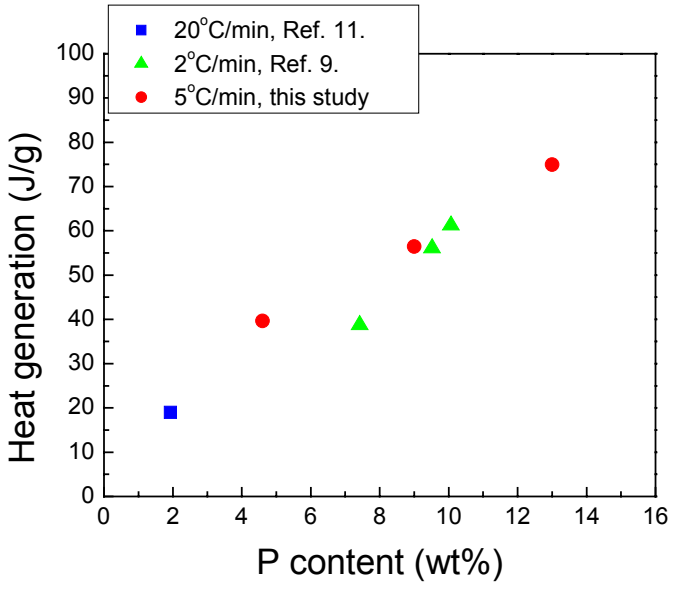


(b)

Fig. 2. (a) DSC curves of 9μm thick Ni-4.6P, Ni-9P and Ni-13P films without Sn heated up to 450°C at a heating rate of 5°C/min and (b) Heat of crystallization deduced from the DSC curves as a function of the P content in the Ni-P layer.

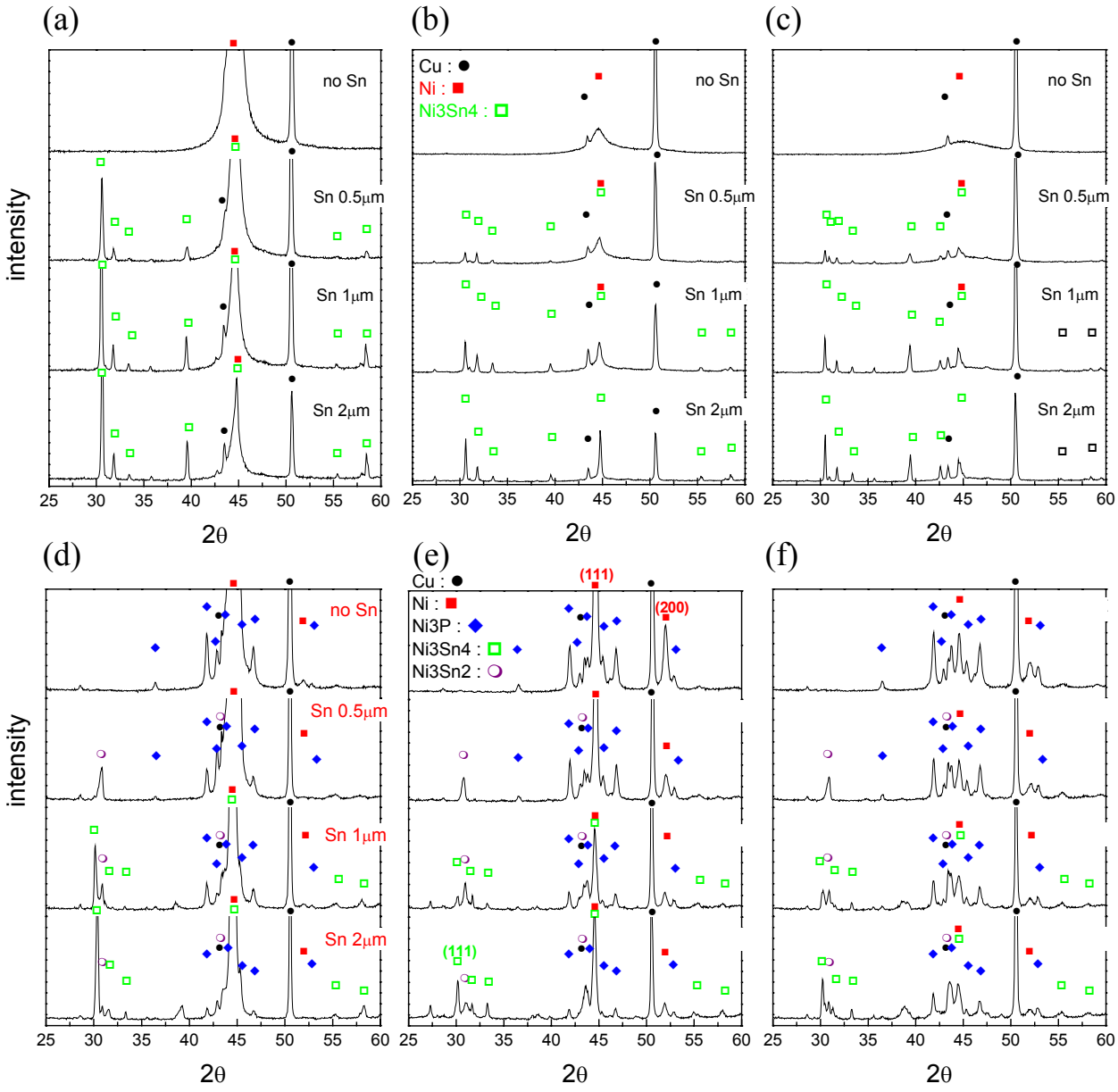


Fig. 3. XRD patterns out of 9μm thick Ni-P films reacted with Sn layers of varying thickness (0.5~2μm) heated up to 300°C in case of (a) Ni-4.6P (b) Ni-9P (C) Ni-13P and heated up to 450°C in case of (d) Ni-4.6P (e) Ni-9P (f) Ni-13P at a heating rate of 5°C/min.

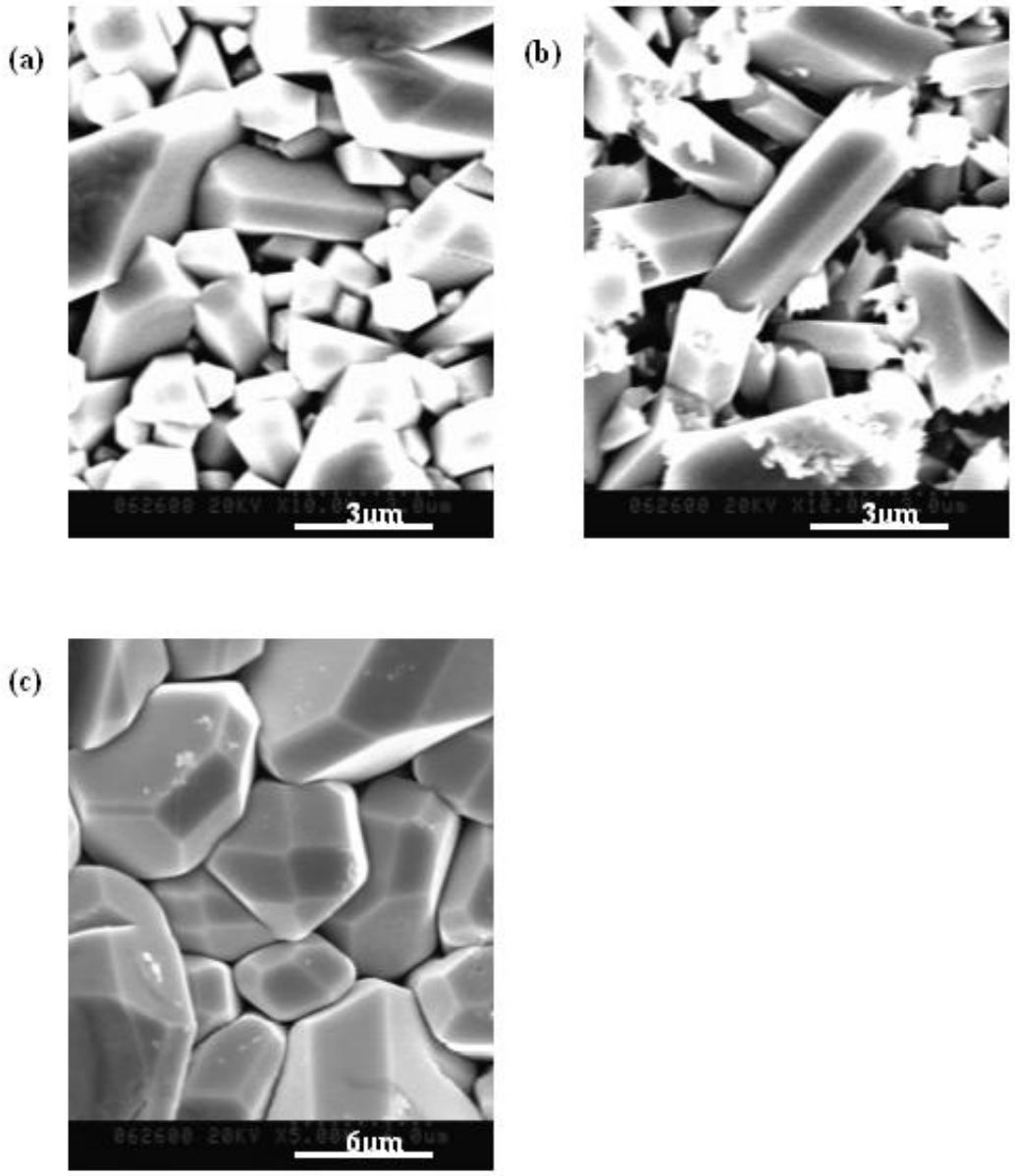


Fig. 4. Morphologies of Ni-Sn IMCs formed at Ni-P/Sn interfaces. (a) $Ni_3Sn_4$ formed at 9μm thick Ni-4.6P reacted with 2μm thick Sn layer heated up to 300°C (b) $Ni_3Sn_4$ formed at 9μm thick Ni-13P reacted with 2μm thick Sn layer heated up to 300°C (C) $Ni_3Sn_2$ formed at 9μm thick Ni-13P reacted with 0.5μm thick Sn layer heated up to 450°C at a heating rate of 5°C/min.

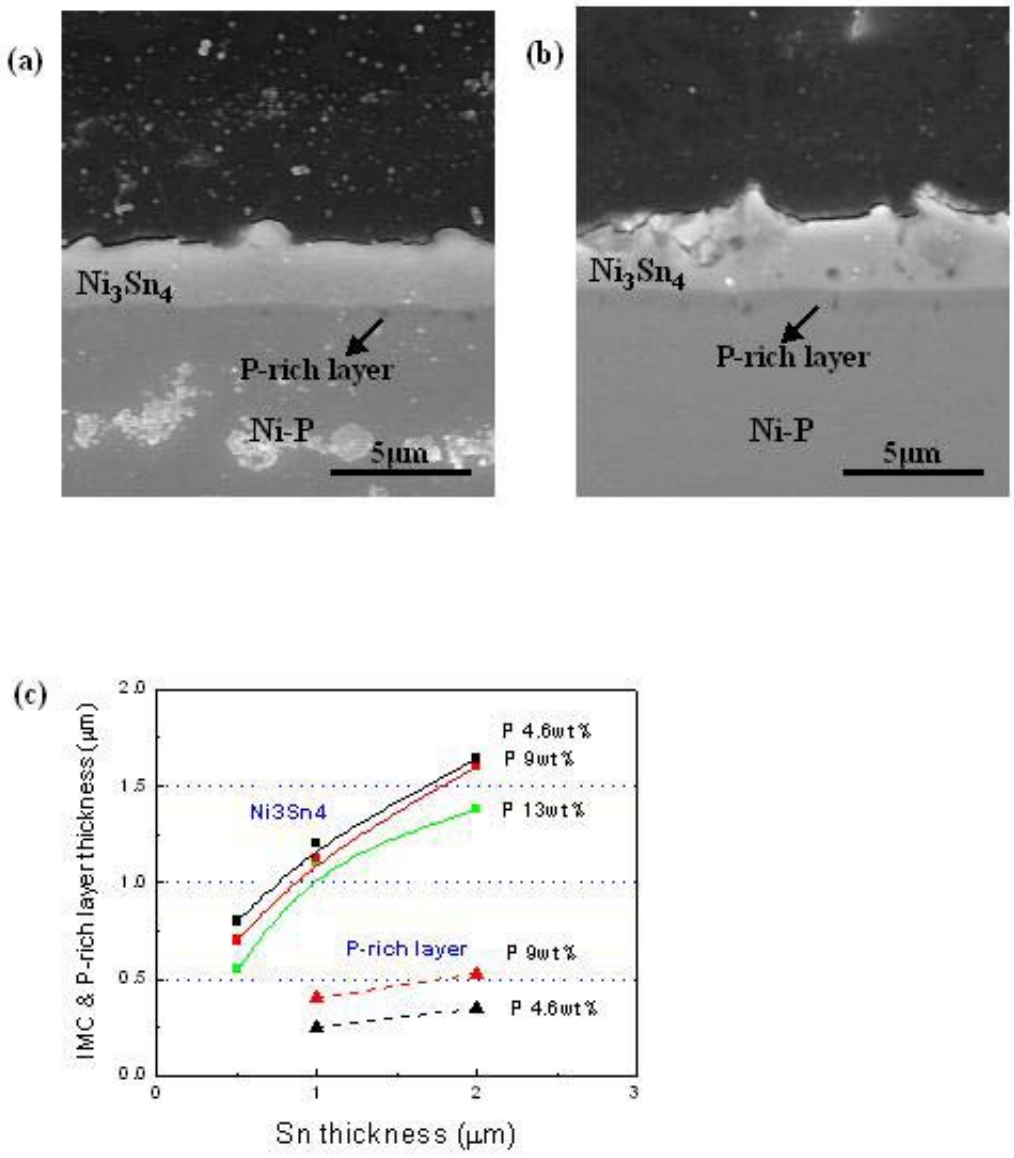


Fig. 5. Cross-sectional SEM micrographs of 9μm thick Ni-P reacted with 2μm thick Sn layer heated up to 300°C at a heating rate of 5°C/min in case of (a) Ni-4.6P and (b) Ni-9P and (C) the average thickness of $Ni_3Sn_4$ and P-rich layer as a function of Sn layer thickness.

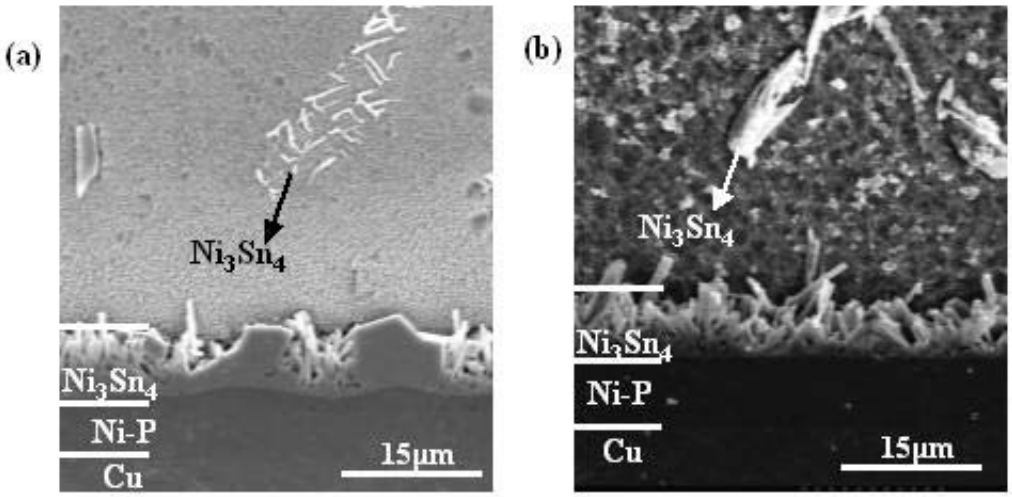


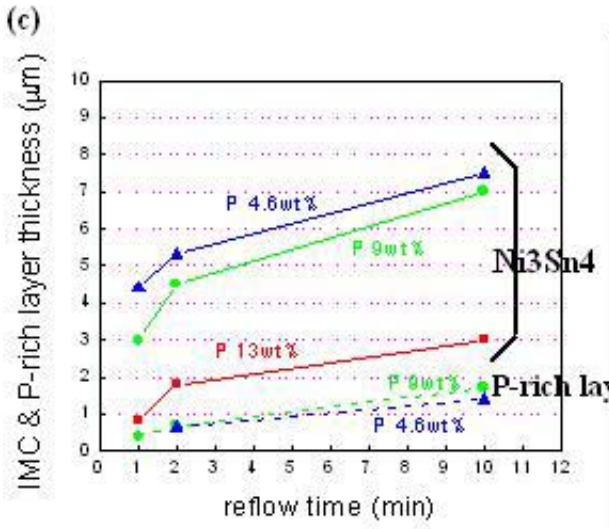


| P % in Ni-P | Reflow time(min) | IMC thickness(μm) |
|---|---|---|
| 4.6wt% | 1 | 4.4 |
| | 2 | 5.3 |
| | 10 | 7.5 (5.5~11) |
| 9wt% | 1 | 3 |
| | 2 | 4.5 (2.5~5.5) |
| | 10 | 7 (5.5~9) |
| 13wt% | 1 | 0.8 |
| | 2 | 1.8 (0.8~5) |
| | 10 | 3 (1.5~6.6) |

Fig. 6. Cross-sectional SEM micrographs of 9μm thick Ni-P reacted with 120μm thick Sn layer reflowed at 250°C up to 10 minutes in case of (a) Ni-9P and (b) Ni-13P and (C) the average thickness of $Ni_3Sn_4$ and P-rich layer as a function of reflow time.